*metals*

MDPI

*Article*

# Stability Investigation of $TiB_2$ Coatings in Molten Zinc Fabricated by Electrophoretic Deposition in Molten Salts

**Jialie Liu [1], Junjie Xu [1], Chuntao Ge [1], Jie Pang [1], Weiliang Jin [2], Geir Martin Haarberg [3] and Saijun Xiao [1,*]**

[1] School of Metallurgy Engineering, Anhui University of Technology, Maanshan 243032, China; 18368829964@163.com (J.L.); 19159358116@163.com (J.X.); 17681250319@163.com (C.G.); pangjie0627@126.com (J.P.)
[2] Department of Metallurgy, Tohoku University, Sendai 980-8579, Japan; jin.weiliang.t6@dc.tohoku.ac.jp
[3] Department of Materials Science and Engineering, Norwegian University of Science and Technology, 7034 Trondheim, Norway; geir.martin.haarberg@ntnu.no
* Correspondence: xiaosaijunzj@yahoo.com

**Abstract:** To enhance the anticorrosion properties of molybdenum metal in liquid zinc, this study successfully fabricated $TiB_2$ coatings on molybdenum substrates via the molten salt electrophoretic deposition technique and investigated their corrosion resistance in molten zinc. Initially, $TiB_2$ nanoparticles with a size ranging from 50 to 150 nm were synthesized using the borothermal reduction method in a molten NaF-$AlF_3$ bath at 1238 K. Subsequently, the electrophoretic deposition experiment was conducted under a cell voltage of 1.2 V (i.e., 0.6 V/cm) for a duration of 1 h in the melt containing $TiB_2$ nanoparticles, resulting in a uniform, continuous, and compact $TiB_2$ coating (35 μm thick) on the molybdenum substrate. Moreover, the corrosion resistance of the $TiB_2$-coated molybdenum metal to molten zinc was tested through continuous immersion. After 120 h of immersion, the $TiB_2$ coating showed no signs of cracking or peeling off, successfully protecting the molybdenum metal substrate from corrosion by molten zinc. The results confirm that the molten salt electrophoretic deposition technique can be used to prepare $TiB_2$ coatings with good resistance to molten zinc corrosion on molybdenum metal.

**Keywords:** molten salt; electrophoretic deposition; molybdenum metal; $TiB_2$ coating; corrosion resistance in molten zinc



**Citation:** Liu, J.; Xu, J.; Ge, C.; Pang, J.; Jin, W.; Haarberg, G.M.; Xiao, S. Stability Investigation of $TiB_2$ Coatings in Molten Zinc Fabricated by Electrophoretic Deposition in Molten Salts. *Metals* **2024**, *14*, 981. https://doi.org/10.3390/met14090981

Academic Editor: Caterina Zanella

Received: 25 July 2024
Revised: 26 August 2024
Accepted: 27 August 2024
Published: 29 August 2024



## 1. Introduction

Molybdenum and its alloys have high melting points, excellent corrosion resistance, and a small coefficient of expansion and are often applied in the field of anticorrosion for liquid metal [1,2]. To enhance their corrosion resistance in liquid metal, researchers have explored two aspects: optimizing the microstructure of molybdenum metal [3,4] and enhancing its surface characteristics [5–7]. Although adjustments to the composition and structure of molybdenum metal can effectively enhance its corrosion resistance to liquid metal, this strategy also inevitably leads to increased complexity in material processing and higher costs [8–10]. Therefore, enhancing the anticorrosion properties of molybdenum metals to liquid metal through the surface treatment technique is a more effective and cost-efficient approach.

Transition metal borides, due to their high melting points, excellent thermal conductivity, and chemical stability at elevated temperatures, are ideal surface coating materials for resisting corrosion by liquid metal [11–14]. Researchers have investigated the corrosion resistance of coatings of transition metal boride such as $ZrB_2$ [15], $TiB_2$-$Al_2O_3$ [16], MoB-CoCr [17], and FeB/$FeB_2$ [18] in molten zinc, achieving satisfactory results. The primary methods currently used for fabricating transition metal boride coatings resistant to molten zinc corrosion include molten salt electrodeposition [15], plasma spraying [19], supersonic flame spraying [20], and boron infiltration treatment [21]. However, these methods are

still limited by the complexity of the process, high equipment costs, and poor coating quality, necessitating further optimization or the development of entirely new coating manufacturing technologies.

In recent years, the authors of this paper have successfully developed a novel method for the fabrication of coatings of transition metal diborides such as $TiB_2$ and $ZrB_2$: molten salt electrophoretic deposition (MS-EPD) [22–25]. This method offers several significant advantages: it features a streamlined process, does not rely on expensive equipment, and yields coatings with dense and high-purity characteristics. This study synthesized nanoscale $TiB_2$ particles via the borothermal reduction of $TiO_2$ in molten NaF-$AlF_3$. Subsequently, by applying cell voltages to the NaF-$AlF_3$ melt containing $TiB_2$ nanoparticles (NPs), a dense $TiB_2$ coating was formed on the cathodic molybdenum metal substrate via the electrophoretic deposition (EPD) process. This paper selected liquid Zn as the media and tested the corrosion resistance of $TiB_2$-coated molybdenum metal substrates against molten zinc. The results indicated that $TiB_2$ coatings, prepared via the EPD technique, can effectively protect the molybdenum substrate from molten zinc corrosion, potentially enhancing the performance of molybdenum and its alloys in extreme environments.

## 2. Materials and Experimental Procedure

### *2.1. EPD of $TiB_2$ Coatings in NaF-$AlF_3$ Molten Salts*

The process of preparing $TiB_2$ coatings by MS-EPD consists of two steps. First, nano-$TiB_2$ was synthesized via borothermal reduction in NaF-$AlF_3$ molten salts. Subsequently, EPD was carried out in the same molten salts containing nano-$TiB_2$ to prepare $TiB_2$ coatings, as illustrated in Figure 1.

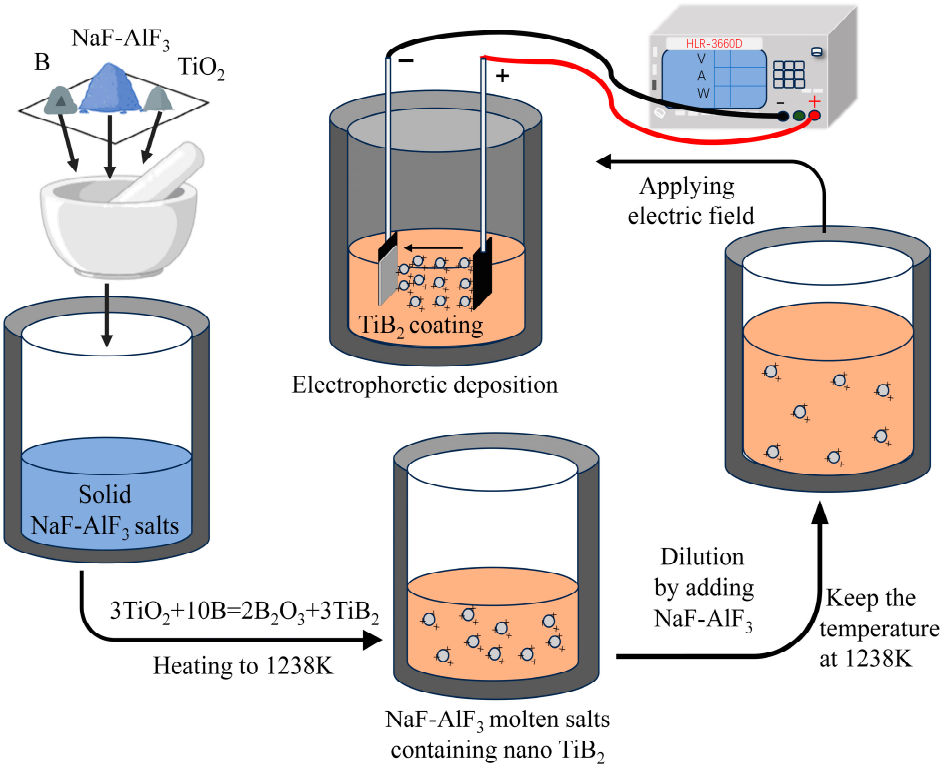


**Figure 1.** Schematic of the process for the synthesis of nano-$TiB_2$ in molten salts and the preparation of $TiB_2$ coatings by EPD.

(1) Synthesis of Nano-$TiB_2$ by Borothermal Reduction in Molten Bath

As shown in Figure 1, the mixture, consisting of NaF (≥99.5%, Aladdin, Shanghai, China), $AlF_3$ (≥98%, Tianjin, Guangfu, Tianjin, China), $TiO_2$ (mean size: 50nm, Shanghai Chaowei Nanotechnology Co., Ltd., Shanghai, China), and B (≥99.9%, Hebei Zhuyan Alloy

Materials Co., Ltd., Xingtai, China), was ground in an agate mortar for around 15 min. Then, it was introduced into a graphite crucible placed in an electric resistance furnace. Afterward, the furnace was heated from room temperature to 1238 K over 100 min and then held for 3 h to fully react and synthesize the $TiB_2$ NPs. Then, a 75 g NaF-$AlF_3$ solid mixture was added to the $TiB_2$ NPs-contained molten salts to dilute them. The molten salts were ready for the EPD experiment after being kept for 1 h.

(2) EPD of $TiB_2$ Coatings

Subsequently, a molybdenum cathode (4 × 2 × 25 mm, ≥99.9%, Haoye Metal Materials Co., Ltd., Shanghai, China) was introduced into the cell to a depth of 15 mm below the surface of the prepared $TiB_2$-containing molten salts, and a graphite anode (6 × 3 × 50 mm) was introduced to a depth of 15–20 mm. The anode and cathode distance was 15 mm, as shown in Figure 1. A DC power supply (HLR-3660D, Henghui, Shenzhen, China) was employed to control the cell voltages. The experimental temperature was 1238 K, and the duration of EPD was 60 min. After the completion of the MS-EPD experiment, the cathode was removed and cleaned by soaking in deionized water for 1 h before being characterized. All EPD experiments were performed under the protection of an argon atmosphere.

### *2.2. Corrosion Resistance Test of $TiB_2$ Coatings in Molten Zinc*

This study utilized high-purity (≥99.99%) zinc, provided by Beijing Jinyuan New Material Technology Co., Ltd. (Beijing, China), acting as the corrosive medium to assess the anticorrosion properties of $TiB_2$ coatings in liquid zinc. Zinc plates were initially cut into 30 × 20 × 5 $mm^3$ dimensions and finely ground using 1000-grit sandpaper. After grinding, the samples were ultrasonically cleaned with acetone and alcohol to clean the surface and then air-dried at room temperature. Then, they were heated and melted in an alumina crucible in a high-temperature furnace. $TiB_2$-coated molybdenum metal samples were held above the liquid zinc surface for 30 s before being slowly immersed into the melt to prevent coating cracking or detachment due to thermal stress. Static corrosion tests were conducted on both $TiB_2$-coated samples and uncoated molybdenum at a temperature of 823 K. The exposure times for $TiB_2$-coated samples in molten zinc were set at 12, 24, 48, 96, and 120 h, while uncoated molybdenum substrates were exposed for 2 and 4 h, respectively. Following the corrosion tests, the samples were removed from the molten zinc, cooled at room temperature, and the solidified zinc adhering to the sample surfaces was preserved for subsequent observation and analysis.

### *2.3. Characterization*

The synthesized $TiB_2$ NPs and cross-sectional morphologies of $TiB_2$ coatings were characterized with a scanning electron microscopy (SEM, model: Tescan Mira3, Brno, Czech Republic) equipped with an energy-dispersive X-ray spectroscopy (EDS) detector (brand: Oxford Instruments, Abingdon, UK). Furthermore, X-ray diffraction (XRD) (Rigaku Ultima IV, Tokyo, Japan operating voltage: 40 kV, current: 40 mA, scanning speed: 10°/min) was employed to analyze the phase composition of $TiB_2$ NPs and $TiB_2$ coatings. In addition, the adhesion strength of the coating to substrate was evaluated using a Revetest Scratch Tester, an automatic device for assessing thin-film adhesion produced by CSM Instruments in Peseux, Switzerland. This device can apply a linear load up to 100 N, with a loading rate of 19.8 N/min and a scratch speed of 1 mm/min, while maintaining a scratch length of 5 mm. Samples subjected to corrosion testing in molten zinc were analyzed using SEM equipped with an EDS detector to assess their surface morphology and composition.

## 3. Results and Discussion

### *3.1. Synthesis of $TiB_2$ NPs and EPD of $TiB_2$ Coatings in NaF-$AlF_3$ Molten Salts*

After the borothermal reduction of titanium dioxide experiment, the molten salts containing $TiB_2$ NPs were recovered when they were naturally cooled down to room temperature. The solidified salts were characterized using XRD and SEM, and the results are presented in Figure 2.

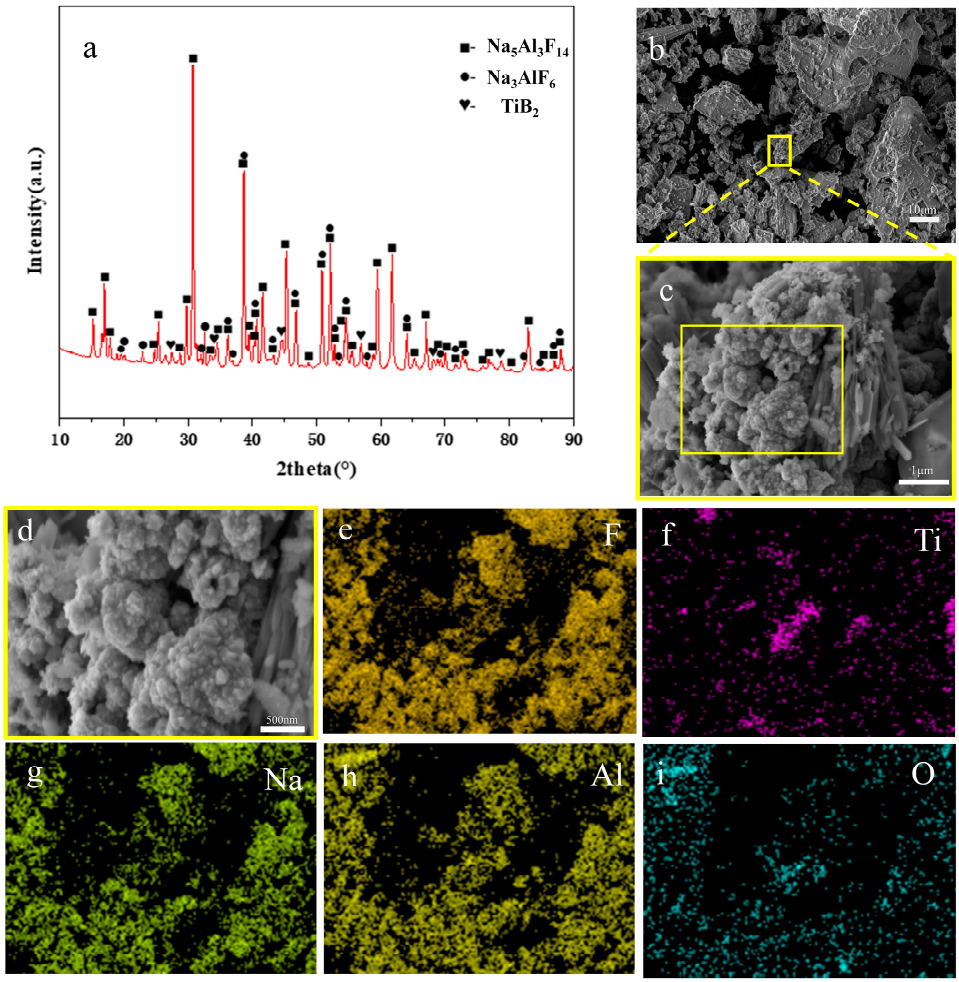


**Figure 2.** XRD result (**a**) and SEM images (**b**–**d**) of solidified salts containing $TiB_2$ NPs. EDS elemental mapping results for F, Ti, Na, Al, and O (**e**–**i**) corresponding to (**b**).

XRD analysis of the NaF-$AlF_3$ solid salt containing $TiB_2$ (Figure 2a) revealed that it mainly consisted of three substances: $TiB_2$, $Na_3AlF_6$, and $Na_5Al_3F_{14}$. Morphologies of the sample revealed that the solid salts consisted of nanoscale particles (Figure 2b–d). Elemental EDS mapping analysis demonstrated the distribution of F, Ti, Na, Al, and O (Figure 2e–i) within the sample. The enrichment of the Ti element, distributed in salts containing Na, Al, and F elements, was observed, and the distribution characteristics of Ti and O indicated those regions enriched with titanium had lower oxygen content. Further magnified SEM characterization of the location enriched with Ti (yellow rectangular area in Figure 2b) revealed the existence of numerous dispersed particles from 50 to 150 nm, as seen in Figure 2c. In conjunction with the XRD results, nanoscale $TiB_2$ particles were successfully synthesized through the borothermal reduction reaction.

Following the successful synthesized $TiB_2$ NPs via borothermal reduction in NaF-$AlF_3$ molten salts, the EPD experiment was conducted by imposing a cell voltage of 1.2 V for 1 h, resulting in a $TiB_2$ coating on the molybdenum cathode. Figure 3a showed the XRD result of the EPDed $TiB_2$ coating on the molybdenum substrate. The result indicated that no other substances existed besides $TiB_2$ and Mo. It confirmed the acquisition of a relatively pure $TiB_2$ coating through the MS-EPD technique. Figure 3b presented a cross-sectional low-magnification image of the $TiB_2$ coating along with the corresponding elemental mapping analysis. The thickness of the $TiB_2$ coating was approximately 35 μm, and the coating was dense, continuous, and uniform, with a smooth surface and no apparent defects. Figure 3c,d demonstrated high magnification and line scan analysis of the area shown in Figure 3b, indicating that the $TiB_2$ coating prepared by MS-EPD was fully dense and pure.

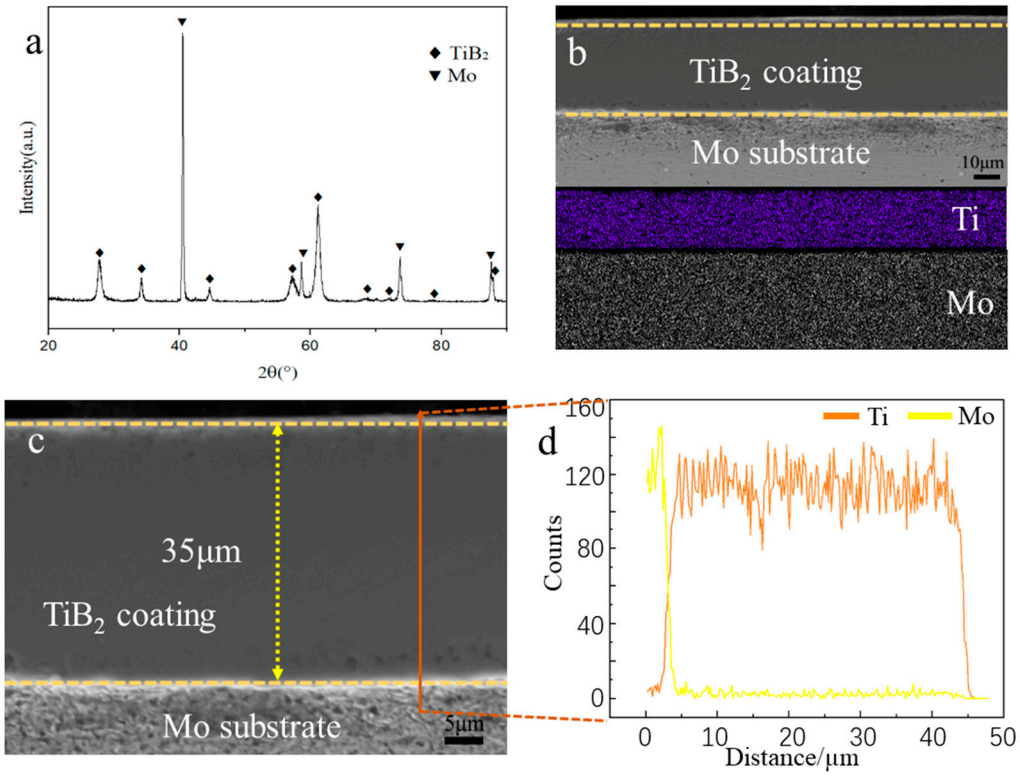


**Figure 3.** Characterization of $TiB_2$ coating on molybdenum substrate prepared by electrophoretic deposition in NaF-$AlF_3$ melt (1 h): (**a**) XRD analysis of the $TiB_2$-coated molybdenum metal. (**b**) Cross-sectional low magnification SEM image with corresponding EDS elemental mapping results for Ti and Mo. (**c**,**d**) Cross-sectional high magnification SEM image with line scan analysis.

The bonding strength between the $TiB_2$ coating and the molybdenum substrate was assessed using a scratch test, with results depicted in Figure 4. A linear load from 0 to 100 N was progressively applied over a 5 mm scratch length. A slight fluctuation in the acoustic signal was observed when the load increased to 37 N. At a load of 44 N, a strong vibration in the acoustic signal occurred, coinciding with the initiation of coating delamination, thereby determining the critical adhesion strength (Lc3) between the $TiB_2$ coating and the molybdenum substrate as 44 N. It confirmed that the $TiB_2$ coating fabricated by MS-EPD exhibited robust adhesion to the molybdenum metal substrate.

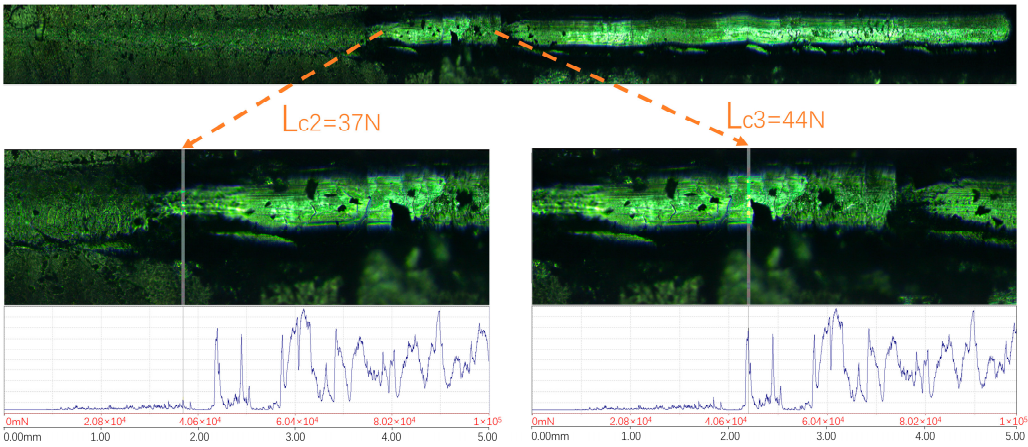


**Figure 4.** Scratch test for the adhesion strength of the $TiB_2$ coating on the molybdenum substrate.

### *3.2. Corrosion Behavior of Uncoated Molybdenum in Molten Zinc*

Utilizing the MS-EPD technique, a $TiB_2$ coating with high adhesion strength and dense structure was successfully fabricated on a molybdenum substrate. Before examining the anticorrosion properties of the $TiB_2$ coating in liquid zinc, this research conducted a systematic investigation into the corrosion behavior of molybdenum metal in molten zinc at 823 K, with soaking durations of 2 and 4 h. After the experiment, detailed testing and analysis were conducted on the molybdenum samples, with results presented in Figures 5 and 6.

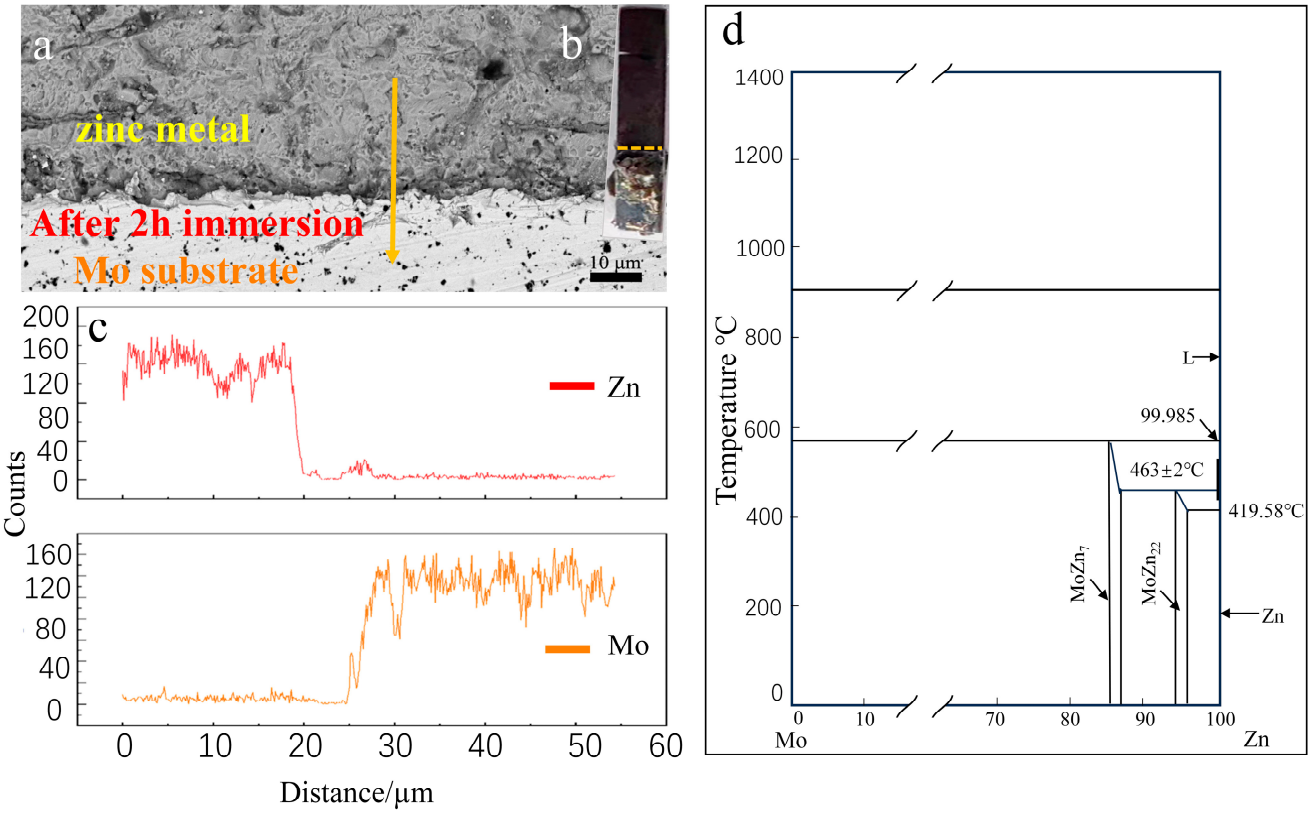


**Figure 5.** Corrosion resistance results of uncoated molybdenum in molten zinc (2 h). (**a**) Cross-sectional SEM image of molybdenum. (**b**) Appearance of molybdenum after immersion in molten zinc. (**c**) Line scan image at the interface between molybdenum and solid zinc. (**d**) Molybdenum–zinc binary phase diagram.

After immersion in liquid zinc at 823 K for 2 h and subsequent cooling, the molybdenum metal exhibited a surface covered with a layer of solid zinc, demonstrating good wettability, as shown in Figure 5b. Analysis of the zinc-coated molybdenum cross-section using SEM (Figure 5a) revealed a transition layer with approximately 8 μm thickness between the molybdenum metal and the surface zinc. EDS line scan analysis (Figure 5c) disclosed the coexistence of molybdenum and zinc elements within the transition layer, indicating erosion of the molybdenum metal by the molten zinc. According to the molybdenum–zinc binary phase diagram (Figure 5d), at 823 K, various types of solid solutions, such as $MoZn_3$ and $MoZn_7$, could potentially form, depending on the concentrations of molybdenum and zinc. This finding confirms that a reactive diffusion occurred between the molybdenum metal and molten zinc, illustrating the inability of molybdenum to resist the corrosive effects of molten zinc.

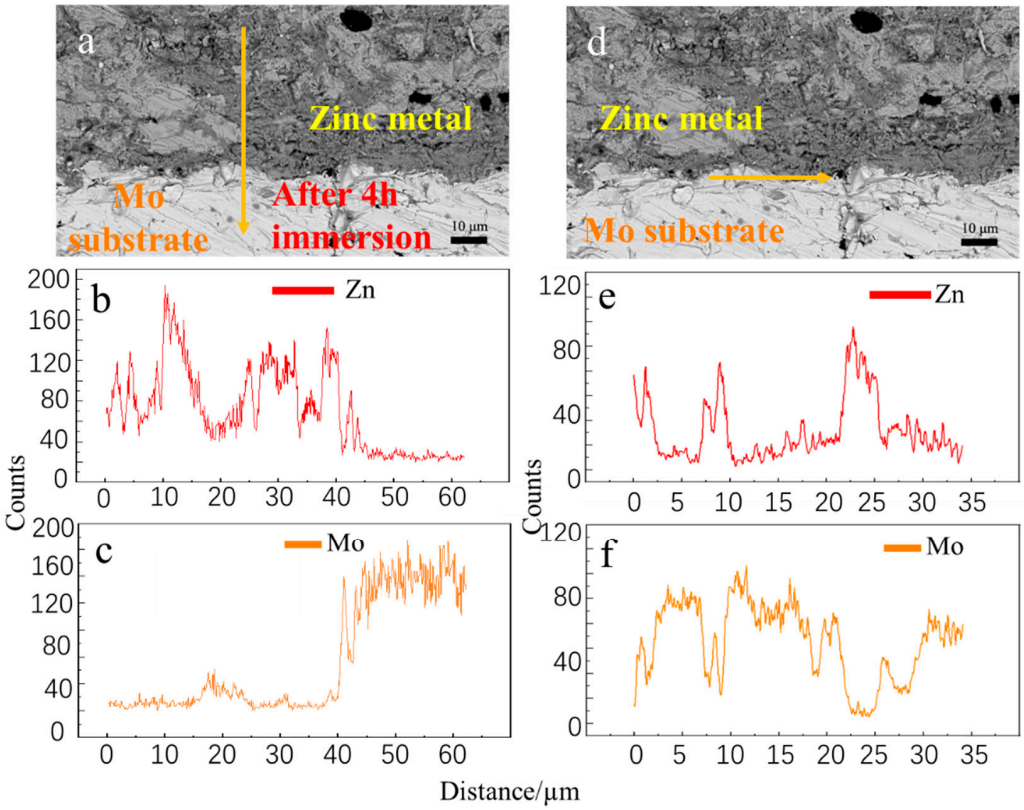


**Figure 6.** Corrosion resistance results of uncoated molybdenum in molten zinc (4 h). (**a**,**d**) are cross-sectional SEM images of the molybdenum metal. (**b**,**c**) are the longitudinal line scan analyses of the interface between the molybdenum metal and solid zinc. (**e**,**f**) are the transverse line scan analyses of the interface between the molybdenum metal and solid zinc.

Given that the cross-sectional images of molybdenum after a 2 h immersion in molten zinc did not clearly reveal the corroded layer, this study extended the immersion to 4 h, with results presented in Figure 6. A transition layer with approximately 20 μm thickness formed at the interface between the molybdenum and solidified zinc, as shown in Figure 6a,d. Longitudinal EDS line scan analysis indicated the coexistence of molybdenum and zinc elements within the transition layer, as depicted in Figure 6b,c, revealing that the degree of molybdenum corrosion significantly increased with the extension of immersion time from 2 to 4 h. Transverse EDS line scans, as shown in Figure 6e,f, revealed fluctuations in the concentration of zinc and molybdenum elements at the interface, likely due to the unevenness of the molybdenum surface and varying diffusion rates between molybdenum and zinc. In summary, since molybdenum forms a solid solution with zinc at 823 K and exhibits relatively weak resistance to corrosion by liquid zinc, the use of protective coatings is particularly important.

### *3.3. Corrosion Behavior of Molybdenum with $TiB_2$ Coatings in Liquid Zinc*

The MS-EPD technique was successfully utilized to form a fully dense $TiB_2$ coating on the molybdenum surface. To thoroughly evaluate the resistance of $TiB_2$ coatings to corrosion in molten zinc, a series of corrosion experiments with varying immersion durations (12, 24, 48, 96, and 120 h) were designed and conducted. Figure 7 demonstrated the corrosion test results for the $TiB_2$-coated samples with immersion times of 12, 24, and 48 h, respectively.

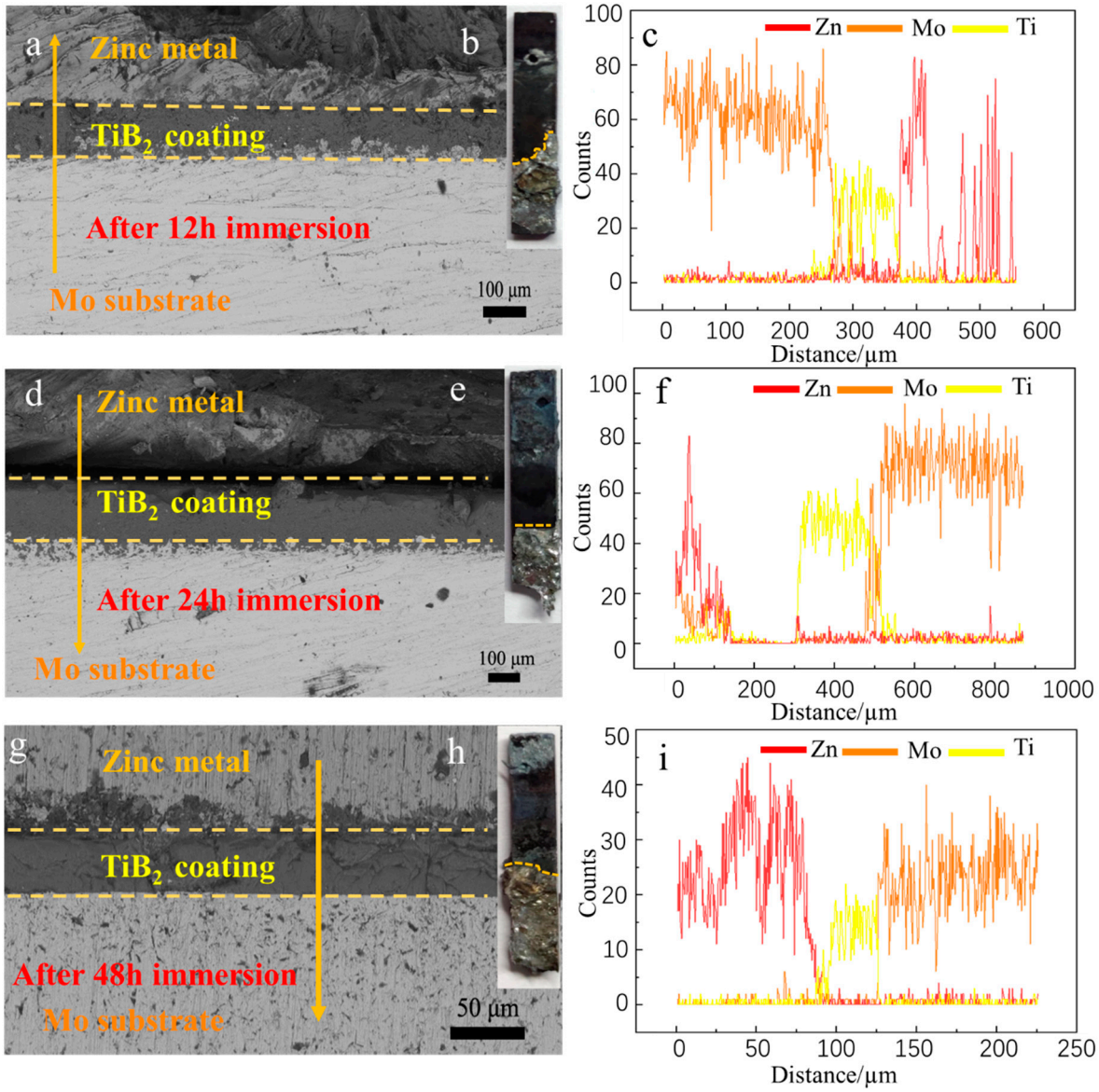


**Figure 7.** Cross-sectional morphologies and EDS line scan results of molybdenum with $TiB_2$ coatings after immersion in liquid zinc for different durations:12 h (**a**–**c**); 24 h (**d**–**f**); 48 h (**g**–**i**).

The photos of the $TiB_2$ coating after being soaked in liquid zinc for 12, 24, and 48 h (Figure 7b,e,h) showed that the surface was uniformly covered by solidified zinc, indicating good wettability between the $TiB_2$ coating and the liquid zinc. SEM images of the cross-section (Figure 7a,d,g) and corresponding line scan results (Figure 7c,f,i) revealed that the $TiB_2$ coating, after being soaked for 12, 24, and 48 h in molten zinc, remained intact without corrosion damage, exhibited no cracks, and maintained strong adhesion to the molybdenum substrate. No new substances were observed at the interface between zinc and the $TiB_2$ coating; only physical adhesion was evident. This suggests that within 48 h, there is no occurrence of a chemical reaction between the $TiB_2$ coating and the liquid zinc, effectively protecting the molybdenum substrate from corrosion.

Furthermore, the soaking time of the $TiB_2$ coating in liquid zinc was extended to 96 h to assess its long-term corrosion resistance. Figure 8a presented the cross-sectional morphology of the $TiB_2$ coating after 96 h of soaking, demonstrating an intact, dense, and continuous structure indicative of excellent anticorrosion. With higher magnification, Figure 8b, c further confirmed that the $TiB_2$ coating effectively protected the molybdenum substrate against long-term erosion by molten zinc, showing no significant signs of

corrosion or damage. Line scan analysis across the cross-section (Figure 8d–f) showed a dramatic decrease in zinc content close to the interface between the $TiB_2$ coating and the zinc, approaching zero. This finding suggests that over the 96h immersion period, zinc did not significantly infiltrate the $TiB_2$ coating via chemical reactions or diffusion, thereby validating the protective efficacy of the $TiB_2$ coating on the molybdenum substrate.

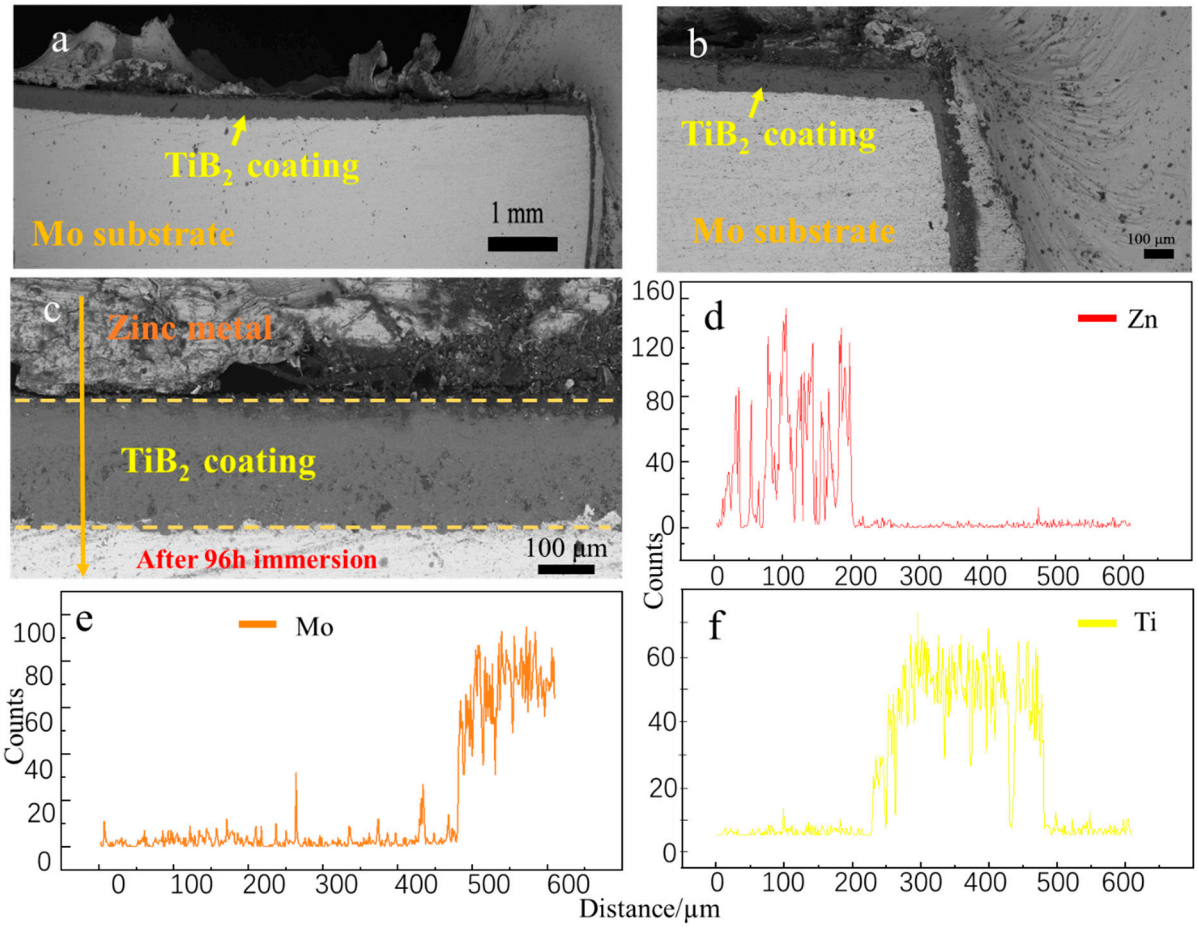


**Figure 8.** Corrosion resistance results of molybdenum with $TiB_2$ coatings in molten zinc (96 h). (**a**) SEM image of the cross-section. (**b**) SEM image with high magnification at the corner. (**c**) SEM image with high magnification on the section. (**d**–**f**) EDS line scan results.

The soaking time of the $TiB_2$ coating in liquid zinc was extended to 120 h to further investigate its corrosion resistance. Figure 9a–c displayed the morphologies of the $TiB_2$ coating cross-section after 120 h of exposure to molten zinc. The results showed that the $TiB_2$ coating remained crack-free and fully dense under a corrosive environment for prolonged exposure time. Line scan results (Figure 9d–f) revealed that at the interface between the $TiB_2$ coating and solid zinc, zinc concentration sharply decreased to zero without any overlapping distribution of titanium elements. These findings confirm that no evident chemical reactions or elemental diffusion occurred between the $TiB_2$ coating and liquid zinc. As shown in Figure 8c, EDS elemental mapping analysis of the cross-section of the $TiB_2$ coating indicated no apparent mixing of molybdenum (Mo), titanium (Ti), and zinc (Zn) at the interface. Therefore, after 120 h of soaking in liquid zinc, it failed to penetrate the interior of the coated $TiB_2$ via chemical reactions or diffusion. It can be concluded that the $TiB_2$ coating, produced via MS-EPD, effectively protects the molybdenum substrate from corrosion by molten zinc.

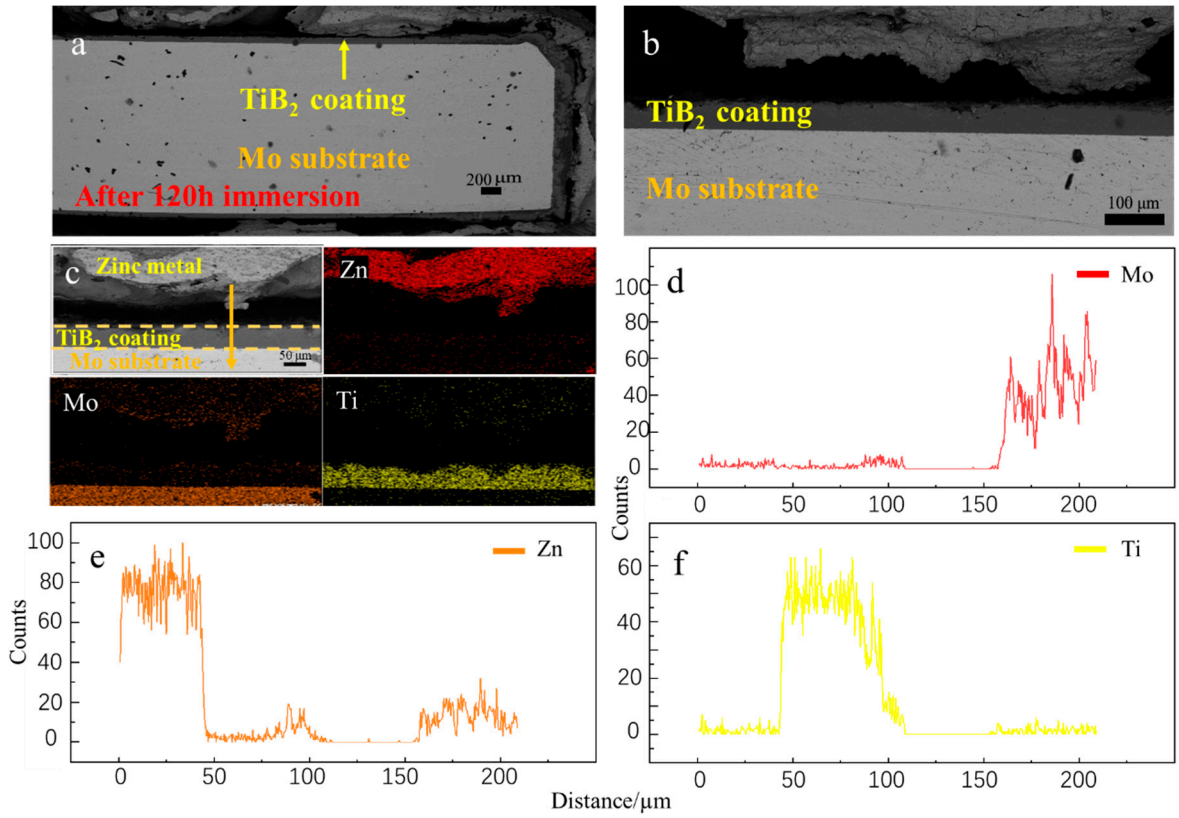


**Figure 9.** Anticorrosion results of molybdenum with the $TiB_2$ coating in liquid zinc (120 h). (**a**) Cross-sectional SEM image. (**b**) Cross-sectional SEM image with high magnification. (**c**) Cross-sectional mapping image. (**d**–**f**) Line scan analysis images.

The $TiB_2$ coating on the molybdenum substrate presents excellent anticorrosion to molten zinc, primarily due to four factors: (1) Experimental results reveal that no chemical reaction occurs between molten zinc and $TiB_2$ at 823 K, resulting in no new substances being formed. Notably, the solubility of $TiB_2$ in liquid zinc at 823 K is relatively low, contributing to the coating's stability and corrosion resistance. (2) The NaF-$AlF_3$ molten salts effectively dissolve $TiO_2$ and $B_2O_3$ [26], enabling the preparation of a low-oxygen $TiB_2$ coating via MS-EPD. This low-oxygen coating prevents intergranular corrosion, thereby enhancing its corrosion resistance. (3) A solid solution reaction between molybdenum and $TiB_2$ [27] forms a metallurgical bond. (4) Additionally, the thermal expansion coefficients of molybdenum and $TiB_2$ are closely matched, corresponding to $4.8 \times 10^{-6}$ $K^{-1}$ [28] and $5.5 \times 10^{-6}$ $K^{-1}$ [29], respectively. These closely matched thermal expansion coefficients and high bonding strength ensure that the coating remains intact during temperature fluctuations. In summary, the $TiB_2$ coating prepared on the molybdenum substrate using MS-EPD technology exhibits remarkable resistance to liquid zinc corrosion. This coating effectively shields the substrate from liquid zinc corrosion, offering robust protection for molybdenum in zinc-rich environments.

## 4. Conclusions

To enhance the anticorrosion properties of molybdenum in liquid zinc, this study successfully fabricated $TiB_2$ coatings on molybdenum substrates using MS-EPD technology and thoroughly investigated the anticorrosion of $TiB_2$ coatings.

1. In the NaF-$AlF_3$ molten salt system at 1238 K, $TiB_2$ particles ranging from 50 to 150 nm were synthesized through the borothermal reduction method. Under a 1.2 V cell voltage, $TiB_2$ NPs migrated within the molten salts and deposited on the molybdenum substrate, forming a dense $TiB_2$ coating with high adhesion strength (Lc3 = 44 N);

2. At 823 K, molybdenum and molten zinc formed a solid solution via reactive diffusion, rendering it unable to resist corrosion. However, the absence of a chemical reaction between $TiB_2$ and molten zinc at 823 K, along with the coating's dense structure and low oxygen content, enables the $TiB_2$ coating to exhibit excellent corrosion resistance after 120 h of immersion, effectively protecting the molybdenum substrate.

**Author Contributions:** Conceptualization, S.X.; methodology, G.M.H. and S.X.; validation, J.L., J.X. and C.G.; formal analysis, J.L., J.X., C.G., W.J. and S.X.; investigation, J.P.; data curation, J.L. and J.P.; writing—original draft preparation, J.L.; writing—review and editing, S.X. All authors have read and agreed to the published version of the manuscript.

**Funding:** This work was supported by the Original Exploratory Program of the National Natural Science Foundation of China (52450012) and the Key Research Project of the Natural Science Foundation of Anhui Provincial Universities (2023AH051094).

**Data Availability Statement:** The raw data supporting the conclusions of this article will be made available by the authors on request.

**Conflicts of Interest:** The authors declare no conflicts of interest.

## References

1. Rivai, A.K.; Takahashi, M. Compatibility of surface-coated steels, refractory metals and ceramics to high temperature lead-bismuth eutectic. *Prog. Nucl. Energy* **2008**, *50*, 560–566. [CrossRef]
2. Abramov, A.V.; Alimgulov, R.R.; Trubcheninova, A.I.; Zhilyakov, A.Y.; Belikov, S.V.; Volkovich, V.A.; Polovov, I.B. Corrosion of Molybdenum-Based and Ni–Mo Alloys in Liquid Bismuth–Lithium Alloy. *Metals* **2023**, *13*, 366. [CrossRef]
3. Wang, B.; Yang, D.; Zhou, Y.C.; Xu, L.J.; Li, Y.P.; Li, X.Q.; Wei, S.Z. Mechanical Properties and Corrosion Behavior in Molten Zinc of Mo–$ZrO_2$ Alloys. *J. Mater. Res. Technol.* **2023**, *25*, 4942–4959. [CrossRef]
4. Wang, B.; Zhou, Y.C.; Yang, D.; Xu, L.J.; Li, X.Q.; Wei, S.Z. Effect of $Al_2O_3$ Particles on the Corrosion Behavior of Molybdenum Alloys in Molten Zinc. *Corros. Sci.* **2023**, *220*, 111266. [CrossRef]
5. Chakraborty, S.P.; Banerjee, S.; Singh, K.; Sharma, I.G.; Grover, A.K.; Suri, A.K. Studies on the Development of Protective Coating on TZM Alloy and Its Subsequent Characterization. *J. Mater. Process. Technol.* **2008**, *207*, 240–247. [CrossRef]
6. Zheng, L.W.; Liu, E.Z.; Zheng, Z.; Ning, L.K.; Tong, J.; Tan, Z. Preparation of alumina/aluminide coatings on molybdenum metal substrates, and protection performance evaluation utilizing a DZ40M superalloy casting test. *Surf. Coat. Technol.* **2020**, *395*, 125931. [CrossRef]
7. Zhang, C.; Liu, E.; Zheng, Z.; Ning, L.; Tong, J.; Tan, Z.; Li, H. Resistance to Molten Superalloy at 1550 °C for Molybdenum Metal Core with a Silica/Silicide Coating. *Coatings* **2021**, *11*, 275. [CrossRef]
8. Wande, C.; Li, T.S.; Xue, D.Z.; Yang, H.J.; Cheng, P.M.; Chen, C.; Sun, Y.J.; Zeng, Y.; Ding, X.D.; Sun, J. Enhancement of the Corrosion Resistance of Molybdenum by $La_2O_3$ Dispersion. *Corros. Sci.* **2021**, *186*, 109469.
9. Xiao, Z.; Liu, J.; Jiang, Z.; Luo, L. Corrosion behavior of refractory metals in liquid lead at 1000 °C for 1000 h. *Nucl. Eng. Technol.* **2022**, *54*, 1954–1961. [CrossRef]
10. Abramov, A.V.; Alimgulov, R.R.; Trubcheninova, A.I.; Zhilyakov, A.Y.; Belikov, S.V.; Volkovich, V.A.; Polovov, I.B. Corrosion of Metals and Nickel-Based Alloys in Liquid Bismuth–Lithium Alloy. *Metals* **2021**, *11*, 791. [CrossRef]
11. Yu, Z.D.; Chen, M.H.; Wang, J.L.; Li, F.J.; Zhu, S.L.; Wang, F.H. Enamel Coating for Protection of the 316 Stainless Steel Against Tribo-Corrosion in Molten Zinc Alloy at 460 °C. *J. Mater. Sci. Technol.* **2021**, *65*, 126–136. [CrossRef]
12. Yadav, K.K.; Guchhait, S.K.; Sunaina; Ankush; Hussain, C.M.; Ganguli, A.K.; Jha, M. Synthesis of Zirconium Diboride and Its Application in the Protection of Stainless steel Surface in Harsh Environment. *J. Solid State Electrochem.* **2019**, *23*, 3243–3253. [CrossRef]
13. Hu, Z.W.; Li, W.G.; Zhao, Y.T. The Effect of Laser Power on the Properties of $M_3B_2$-Type Boride-Based Cermet Coatings Prepared by Laser Cladding Synthesis. *Materials* **2020**, *13*, 1867. [CrossRef]
14. Wang, G.C.; Chong, X.Y.; Li, Z.L.; Feng, J.; Jiang, Y.H. Design of $Fe_2B$-Based Ductile High Temperature Ceramics: First-Principles Calculations and Experimental Validation. *Ceram. Int.* **2022**, *48*, 27163–27173. [CrossRef]
15. Wang, Q.; Zhang, J.; Zhang, L.; Liu, H.; Zeng, C. Stability Investigation of Electrodeposited Zirconium Diboride Ceramic Coatings in Molten Zinc. *Mater. Corros.* **2019**, *70*, 492–502. [CrossRef]
16. Lv, Y.H.; Wu, X.S.; Liu, Y.F.; Wu, Z.J. Preparation and Liquid Zinc Corrosion Resistance of $Al_2O_3$-$TiB_2$ Composite Ceramic Coating. *China Surf. Eng.* **2011**, *24*, 30–33.
17. Zhang, J.F.; Deng, C.M.; Song, J.B.; Deng, C.G.; Liu, M.; Zhou, K.S. MoB–CoCr as Alternatives to WC–12Co for Stainless Steel Protective Coating and Its Corrosion Behavior in Molten Zinc. *Surf. Coat. Technol.* **2013**, *235*, 811–818. [CrossRef]
18. Tsipas, D.N.; Triantafyllidis, G.K.; Kipkemoi, J.; Flitris, Y. Thermochemical Treatments for Protection of Steels in Chemically Aggressive Atmospheres at High Temperatures. *Mater. Manuf. Process.* **1999**, *14*, 697–712. [CrossRef]

19. Lv, J.S.; Li, W.; Li, T.; Guo, L.X.; Fu, Y.Q.; Li, J.C.; Zhang, J.C.; Zhang, Y.L. Ablation behavior of high-entropy boride (Hf-Zr-Ta-Ti)B2 coating fabricated via supersonic atmospheric plasma spraying for carbon/carbon composites. *Eng. Proc.* **2024**, *270*, 111137. [CrossRef]
20. Li, K.Z.; Liu, G.X.; Zhang, Y.L. Ablation properties of HfB2 coatings prepared by supersonic atmospheric plasma spraying for SiC-coated carbon/carbon composites. *Surf. Coat. Technol.* **2019**, *357*, 48–56. [CrossRef]
21. Liu, Y.; Liu, X.Y.; Lai, C.; Ma, J.; Meng, X.F.; Zhang, L.; Xu, G.G.; Lu, Y.W.; Li, H.Y.; Wang, J.S.; et al. Boriding of tungsten by the powder-pack process: Phase formation, growth kinetics and enhanced neutron shielding. *Int. J. Refract. Met. H* **2023**, *110*, 106049. [CrossRef]
22. Jin, W.L.; Xiao, S.J.; Kou, Q.; Ding, D.S.; Zhang, J.; Fang, X.H.; Ge, C.T.; Zhong, C.; Zhu, H.M.; Haarberg, G.M. Preparation of Diboride Coatings by Electrophoretic Deposition in Nanoparticle-Containing Molten Inorganic Salts. *Mater. Lett.* **2021**, *306*, 130908. [CrossRef]
23. Pang, J.; Kou, Q.; Ge, C.T.; Xie, L.L.; Jin, W.L.; Qi, W.Q.; Zhang, J.; Zhu, H.M.; Xiao, S.J. Electrophoretic deposition of $ZrB_2$ coatings in NaCl-KCl-$AlF_3$ melt containing synthesized $ZrB_2$ nanoparticles. *J. Am. Ceram. Soc.* **2023**, *106*, 5147–5156. [CrossRef]
24. Zhang, J.; Pang, J.; Jin, W.L.; Chu, S.J.; Haarberg, G.M.; Xiao, S.J. Production of $TiB_2$ coatings on graphite substrates by electrophoretic deposition in NaF-$AlF_3$ melt. *Process Appl. Ceram.* **2023**, *17*, 9–13. [CrossRef]
25. Zhang, J.; Chu, S.J.; Jin, W.L.; Cai, F.; Zhu, H.M.; Xiao, S.J. Fabrication of $TiB_2$ coatings by electrophoretic deposition of synthesized $TiB_2$ nanoparticles in molten salts. *J. Mater. Res. Technol.* **2022**, *18*, 2451–2457. [CrossRef]
26. Sørlie, M.; Øye, H.A. *Cathode in Aluminium Electrolysis*; Aluminium-Verlag Marketing & Kommunikation GmbH Press: Düsseldorf, Germany, 2010.
27. Verkhoturov, A.D.; Egorov, F.F.; Podchernyaeva, I.A.; Smolin, M.D.; Timofeeva, I.I.; Isaeva, L.P.; Chiplik, V.N. Characteristics of coating formation on steel during electric-spark alloying with heterophase $TiB_2$+Mo materials in air. *Powder Metall. Met. Ceram.* **1983**, *22*, 993–997. [CrossRef]
28. Petukhov, V.A.; Chekhovskoi, V.Y.; Zaichenko, V.M. Thermal Expansion of Molybdenum. *High Temp.* **1977**, *14*, 724–728.
29. Pierson, H.O.; Randich, E. Titanium Diboride Coatings and their Interaction with the Substrates. *Thin Solid Films* **1978**, *70*, 119–128. [CrossRef]